Journal of Fundamental and Applied Sciences

Research Article

ISSN 1112-9867

Available online at http://www.jfas.info

QUANTIFYING THE EFFECT OF GREEN-ROOF AND URBAN GREEN INFRASTRUCTURE RATIO ON URBAN HEAT ISLAND MITIGATION - SEMI-ARID CLIMATE

S. Sahnoune[1*], N. Benhassine[2], F. Bourbia[2], H. Hadbaoui[2]

[1]Institute of Sciences & Technologies, University AbdelHafid Boussouf, Mila, Laboratory of Bioclimatic Architecture and Environment (ABE) Algeria

[2]Laboratory of Bioclimatic Architecture and Environment (ABE), Department of Architecture, University -Salah Boubnider- Constantine 3, Algeria

Received: 31 May 2020/ Accepted: 06 October 2020 / Published online: 01 January 2021

ABSTRACT

Green Roof (GR) is one of the most applied strategies to Mitigate Urban Heat Island (UHI) recommended for sustainable cities. This research aims to examine and evaluate the effect of the GR/UGI ratio on UHI mitigation, creating Urban Cool Island (UCI). The study was carried out at Constantine, situated in the East part of Algeria, characterized by a semi-arid climate with high summer solar radiation intensity. An urban climate analysis was conducted during the hottest period of the year by means of remote sensing data using ArcGIS 10.2 platform. The results displayed that vegetation, urban density, and topography strongly affect UHI. Furthermore, other finding results in this research show that fixing GR/UGI ratio (with 0.0063 reduced the average air temperature by 1.24°C) in a large-scale urban area, can reduce the surface temperature by 4.00 degrees of the studied area.

Keywords: Urban Heat Island (UHI); Green-Roof Ratio/Urban Green Infrastructure (GR/UGI); Urban Cool Island (UCI)

Author Correspondence, e-mail: s.sahnoune@centre-univ-mila.dz

doi: http://dx.doi.org/10.4314/jfas.v13i1.12

1. INTRODUCTION

The Urban heat island (UHI) effects are a result of both natural and human factors mainly related to the characteristics of cities [1] like, recent urbanization marked by important changes in the surface covers and in the built morphology, which causes a change in the urban microclimate.

The current urban built environment, characterized by low urban ventilation and high urban density accentuated by the presence of flat bitumen roofs [2,3]. The latter represents the most exposed elements and the hottest thermal infrared images of urban areas [4]. These contribute to the increasing in air temperature, one of the main factors that have a significant increase in the energy demand of buildings and amplified the use of air conditioning. The UHI can intensify climate change and introduce negative effects, like average global temperature (global warming), changes in rainfall patterns, lead to severe water shortages and/or flooding.

Surface UHIs are measured based on land surface temperature (LST) and tend to be strongest during the day due to the radiation from the sun [5]. LST has been recognized as one of the most important parameters in understanding the urban thermal environment and its dynamics based on the use of satellite images [6,7]. Numerous studies have been conducted to investigate the spatial variation of LST using remote sensing as an important tool for UHI studies [8-12]. Meanwhile, there have been many studies focusing on the correlation between LST and remote sensing indexes such as normalized difference vegetation index (NDVI) and normalized difference water index (NDWI) [13,14]. They have shown their cooling effect on LST acting as cool islands. Besides, improve the capacity of these indexes (or exploit the positive ones) by making the appropriate adjustments and changes to mitigate UHIs are mainly recommended.

To mitigate UHI several strategies have been proposed, developed, and implemented ranged from technological options strategies to behavior change at the individual level [15-19]. Nevertheless, planting is one of the most applied mitigation measures [20].

In general, the air temperature in green areas is cooler than non-green sites in hot months. This fact was confirmed by many research studies on the temperature of parks and forest cover [21]. Several studies have confirmed that this so-called “oasis” shows Cool Island (CI)

effect [22,23]. In some environments such as arid, semi-arid, arctic, and subarctic, cities have been reported as CI (negative UHI) during certain times of the day or during particular seasons [24,25].

The potential cooling benefits of vegetation are increasingly being exploited in rooftop applications. Green roofs have multiple benefits for the urban environment. It has been recognized as an effective sustainable design tool mitigating UHI effects on different scales [26,27] and different urban morphologies [28,29]. Sahnoune and Benhassine [30] investigate the effect of Green Roof/Urban Green Infrastructure (GR/ UGI) ratio on reducing the ambient temperature on the micro-scale in Constantine city, situated in the East part of Algeria (latitude 36°17' N and longitude 6°37' E) with ENVI-met 4.0 software. A comparative-probabilistic approach based on four scenarios of green-roof models has been used. After exploring the results, the 0.0063 ratio has reduced the average air temperature of 1.24°C during the day-time.

To date, plenty of research has investigated the effect of green spaces within cities on UHI mitigation. While few studies have investigated the effect of GR and UGI ratio on UHI mitigation to create UCI; this research requires greater comprehension and employs remote sensing data in investigating surface temperatures of cities in semi-dry environments on a large scale.

In continuance of the previous study of the GR/UGI ratio effect on UHI, we aim in this paper to analyze the effect of 0.0063 ratio that reduces 1.24°C on UHI moderation on a large urban scale of Constantine city. Initially, we classify and map the Land Surface Temperature (LST) of the hottest period of the year using Landsat 8. Besides, we analyze and map the correlation of studied urban variation with LST including the Normalized Difference Vegetation Index (NDVI), Normalized Difference built Index (NDBI), and topography. Then, we identify the hot-spots according to the tall residential buildings with bitumen-flat roofs. Finally, we evaluate the large-scale effect of GR/UGI ratio (0.0063 reduces 1.24°C) on UHI moderation, in creating UCI.

2. METHODOLOGY

The UHI occurs on different scales of the city: micro-scale, local-scale, and mesoscale. Three types of UHI are distinguished: The Urban Canopy Layer heat island (UCL); Urban Boundary Layer heat island (UBL) and UHI surface and sub-surface UHI [31].

This study aims to evaluate the effect of the GR/UGI ratio on UCL by means of LST. To achieve this objective, a series of measurements were done at Constantine city, using the Landsat 8 data Operational Land Imager (OLI) and Thermal Infrared Sensor (TIRS), and the Geographical Information System (GIS).

The Landsat 8 OLI-TIRS recorded the data of the hottest daytime from the U.S Geological Survey (USGS) on July 15, 2015, at 10.06 am. Path 193/row 35, and azimuth = 120.39°, elevation = 65.62°. The spatial resolution of the thermal image is 100 m per pixel. The band 11 (thermal infrared band) was used to retrieve the land surface temperature.

The GIS system and Landsat 8 data could provide and map the geographical information due to the Arc-GIS software. The latter is the main platform for GIS; it includes a collection of integrated applications counting Arc-Map, Arc-Catalog, and Arc-Toolbox.

2.1. Study area

As cited before, the investigation was conducted on six urban agglomerations of Constantine (at latitude 36 °17' N and longitude 6 ° 37' E and an altitude of 574m, covering an area of 780.48 km) as shown in (Fig.1), characterized by semi-arid climate. Hot and dry summer goes from June to September, and cold winter from October until March. The absolute highest air temperature recorded in the city is 38.6 °C in July for the period of (2005-2014).

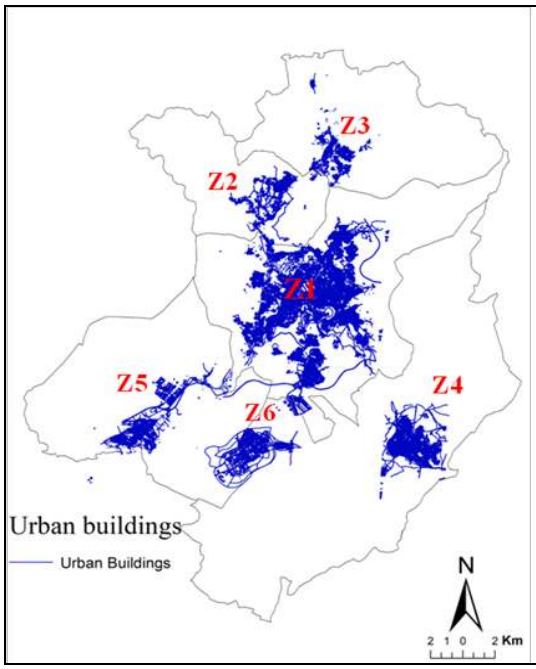

Different urban characteristics of zones

Zones	Location	Urban characteristics
Z1 Constantine-city	The center	-Irregular topography extended on 2 rocky plateaus, which divide the regions in 2 part separated by deep gorges where the river flows. -The whole city composed by a very dense urban structure (residential and industrial areas) with scarce vegetation. - limited by 2 big forest (*Djebel Ouahch* and *El Meridj*) known by their density of *ever* green oak and cypress trees.
Z2 Hamma Bouziane	North-West of Z1	-Agricultural and vegetation areas with a small percentage of building with bitumen-flat roofs (rural area).
Z3 Didouche Morad	North-East of Z1	-Residential area and sparse vegetation.
Z4 El Khroub	South-East of Z1	-Flat site -Residential area and sparse vegetation.
Z5 Ain Smara	South-West of Z1	-Agricultural and mountainous area. Surrounded by forest Chattaba
Z6 Ali Mendjeli	Between Z4 and Z5	-It can be detected as new zone Z6 Typically, residential area, characterized by lack of vegetation.

Fig.1. The map showing the investigated area, and the table summarized the different urban characteristics of studied zones

2.2. Data processing and analysis

2.2.1. LST measurements

As cited before, several studies have characterized the effect of UHI in cities by measuring LST. Additionally, the LST is supposed to correspond more closely with the UCL heat islands [32]. Besides, the UHI could be analyzed by measuring the vegetation and the built-up areas with the Normalized Difference Vegetation Index (NDVI) and the Normalized Difference Built-up Index (NDBI) as indicators.

The NDVI is used in LST estimation to quantify the presence of vegetation and to infer general vegetation conditions [33]. Its value ranges from -1 to1 [34]. NDVI is defined as the ratio of the difference between near-infrared and red reflectance to their sum [35,36] as follows;

$$NDVI = \frac{(NIR - Red)}{(NIR + Red)} \qquad (1)$$

The NDBI maps the urban built-up areas [37]. Its values are represented as a ratio ranging from -1 to 1. NDBI is calculated with the bands 5 and 4 that correspond to Near-infrared and short-wave infrared respectively by the following equation;

$$NDBI = \frac{(SWIR - NIR)}{(SWIR + NIR)} \quad (3)$$

For retrieving LST, a Mono-window algorithm was created and applied through a raster calculator in ArcGIS 10.2 based on the metadata file (MLT) (Table1). The following steps explain the calculation of LST;

Step 1: Estimation of Top of Atmospheric (TOA) Spectral Radiance of thermal Band 11

The LST consists of quantized and calibrated Digital Numbers (DN) representing the multispectral image data (USGS). The following equation was used to rescale the DN values of thermal band 11 into TOA values using the radiance rescaling factors in the MTL file [38].

$$L\lambda = \text{MLQcal} + \text{A} \quad (3)$$

Step 2: Estimation of Brightness Temperature (BT) of thermal Band 11 in Celsius

The thermal band 11 was converted from spectral radiance to top of atmosphere brightness temperature (BT) using the thermal constants in the MTL file as follows:

$$\text{T} = \frac{\text{K2}}{(\text{Ln}(\text{K1}/\text{LA} + 1)) - 272.15} \quad (4)$$

Step 3: Estimation of Fractional Vegetation Cover (FVC) for an image using NDVI

The FVC describes the vegetation proportion by scaling NDVI according to $NDVI_{min}$ and $NDVI_{max}$ by the following equation;

$$PV = \frac{NDVI - NDVImin}{NDVImax - NDVImin} \quad (6)$$

Step 4: Estimation of Land Surface Emissivity (LSE)

Land Surface Emissivity (LSE) was estimated using the fractional Vegetation cover (FVC) [39]. The formula is;

$$E = 0.04PV + 0.986 \quad (6)$$

Step 5: Estimation of LST

The Land Surface Temperature (LST) was calculated as follows [40];

$$LST = \frac{BT}{1} + W \times \left(\frac{BT}{p}\right) \times Ln(E) \quad (7)$$

Table1. Metadata of the sensor Landsat 8 OLI-TIRS

	Metadata file
M_L	Band-specific multiplicative rescaling factor.
A_L	Band-specific additive rescaling factor.
Q_{cal}	Quantized and calibrated standard product pixel values of the BAND10 and the BAND 11
BT	Brightness temperature (K).
L_λ	TOA spectral radiance (Watts/ m^2 .srad .μm).
K1	480.8883 Kelvin, of the band 11
K2	1201.1442 Kelvin, of the band 11
W	Wavelength of emitted radiance
P	Air vapor partial pressure = h× c/ s (1.423×10 ^-2m. k) with P=14380.
h	Planck's constant (6.626×10 ^-34J/K)
s	velocity of light (2.998 ×10 ^8m/s)
E	Emissivity

2.2.2. Effect of NDBI, NDVI and topography on LST

In this part, we analyze and map the correlation of studied urban variation with LST, including NDVI, NDBI, and topography.

The correlation between NDVI and NDBI with LST was analyzed. Following this, 10 sample points randomly of LST, NDVI, and NDBI images were classified, and the statistical association of NDBI and NDVI with LST was calculated with the Pearson's correlation coefficient respectively.

To evaluate the influence of topography, a Digital Elevation Model (DEM) derived from the Geological Survey (USGS) ASTER global was calculated with an absolute vertical and horizontal accuracy of 90 and 1m respectively. In DEM raster, each cell has a value corresponding to its elevation. Based on the DEM, a hill shade was calculated in degrees using the spatial analyst tool (Arc-GIS) with specifying the sun elevation, and the azimuth angle in the corresponding fields.

Then, we overlapped the high and low DEM pixel values with the values of raster shading ranged from 0 to over 180. The Hill shade gives the hypothetical insolation of a surface by determining illumination values for each cell in a raster. Hence the Hill shade corresponds to differences in the energy balance of areas with different topography [41].

2.2.3. Detection of hot-spots in studied urban areas

The hot-spots were identified according to the tall residential buildings with bitumen-flat roofs. Therefore, we have used a uniform grid, the tall residential buildings with bitumen-flat roofs shape-file, and the LST of the band 11 shape-file.

First, the shape-file of tall residential building with the bitumen-flat roof was converted to a set of polygons, then to a set of points. The values of LST were transformed into another set of points, where each point representing a distinct temperature value. Thus, a new field of temperature values named raster-value was listed in the attribute table, having each point of a tall residential buildings with bitumen-flat roof linked to its corresponding temperature value.

Secondly, the new raster-values of LST were classified and joined in a uniform grid of pixels representing a $1km^2$ square area.

Finally, the hot-spots were identified with an unsupervised classification of LST raster values. We have used a threshold higher or equal to 29°C as the comfort temperature [42]. The comfort temperature of the region of Constantine is ranged between 18°C in winter and 29°C in summer.

2.2.4. Creation of Urban Cool Islands (UCI)

Urban greenery has been proposed as an effective measure to mitigate UHI [43, 44, 45, 46], Creating UCI. The present part quantifies firstly the UGI density and then evaluates the large-scale effect of GR/UGI ratio on UHI.

Supervised classification of NVDI (Fig.2) on three classes (dense vegetation, sparse vegetation, and no vegetation) was performed. Each class was converted to polygon, and its areas were calculated from the attribute table.

The UGI density is defined by the following equation of [47];

$$UGI\ Density = \frac{Av}{Ae} \qquad (8)$$

Where;

(Av): the area of UGI.

(Ae): the total area of the calculation perimeter.

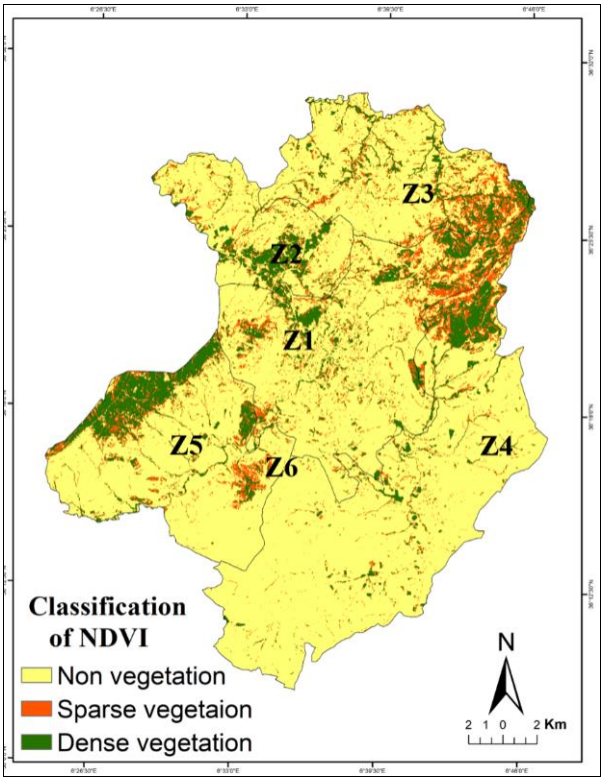

Fig.2.A supervised classification of NDVI

Furthermore, the effect of the GR/UGI ratio of 0.0063 on UHI moderation was evaluated using the Arc-GIS system resulting in (UCI) data. GIS system has been proved to be an important supporting platform for urban thermal analysis able to manage and improve the GR function [48, 49]. The following steps explained the calculation of UCI;

First, we used the shapefile of hot-spots calculated in the previous section.

Secondly, we exported and clipped the shapefile of tall residential buildings with bitumen-flat roofs according to the hot-spots.

Third, we calculated the ratio of bitumen-flat roofs area to the total grid area of the studied zones. The finding results of the calculated ratios are summarized in (Table 2).

Finally, we used the ratio of (GR/UGI) of 0.0063 reduces 1.24°C [30] and tried to calculate the UCI temperature for each zone using the rule of three, which is a particular case of the cross-multiplication with the following equation:

The ratio **0.0063** ⟶ **1.24°C**

The ratio (**Abf/Ac) of (Zone x**) ⟶ $\mathbf{T°_{UCI}}$?

$$T° UCI = \frac{(Ratio \frac{Aft}{Ac} \times 1.24°C)}{(0.0063)} \quad (10)$$

Where;

(Abf): the bitumen-flat roofs area.

(Ap): the total grid area of each zone.

Table 2. Ratios of studied zones

Zones	Area of bitumen- flat roofs *(Abf)*, (m^2)	Total grid area *(Ap)*(m^2)	Ratio of *Abf/AC*
Z1	633283.16	61000000	0.0103
Z3	91339.90	6000000	0.0152
Z4	512590.48	17848034.13	0.0287
Z5	137369.91	11703517.89	0.0117
Z6	503617.39	140000000	0.0359

As mentioned above, the Z2 is not listed in the (Table2), because it was below the 29°C threshold and devoid of tall residential buildings with bitumen-flat roofs as illustrated in (Fig.3).

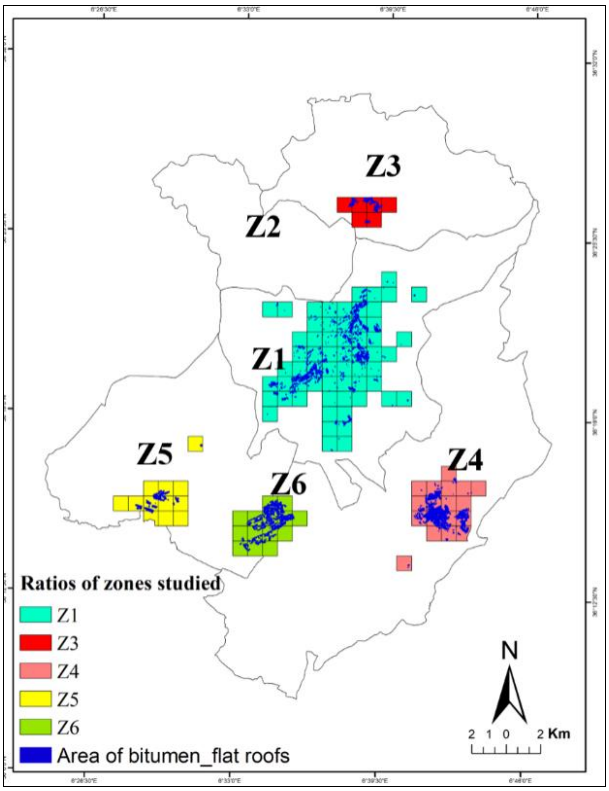

Fig.3. The map showing the ratios of zones studied

The new raster values of UCI temperature were added on each pixel of the grid corresponding to the decrease of temperature on each zone, respectively. As a result, the unsupervised classification of these values identified the Urban Cool Islands (UCI) of the studied area.

3. RESULTATS AND DISCUSSION

3.1. Spatial distribution of LST

The LST map of the studied area is represented in (Fig.4), with values ranged from 26, 6°C to 45°C. At Constantine-city Z1, the urban area is a mixture of building mass and vegetated surfaces. The topography of the city has a great effect on the microclimate [50], which consequently influences the LST of the city, with a medium temperature of 32°C to 36°C showed with light blue. However, the surrounding urban areas characterized by densely-populated [51], urban landscape of asphalt, brick, metal and dark rooftops soaks-up an enormous amount of energy from sunlight reflecting even more light a densely built-up areas [52, 53] such as Z3, Z4, Z, and Z6. They have marked a higher LST reaching 45°C with values ranged from 40°C to 45°C displayed with orange and red color.

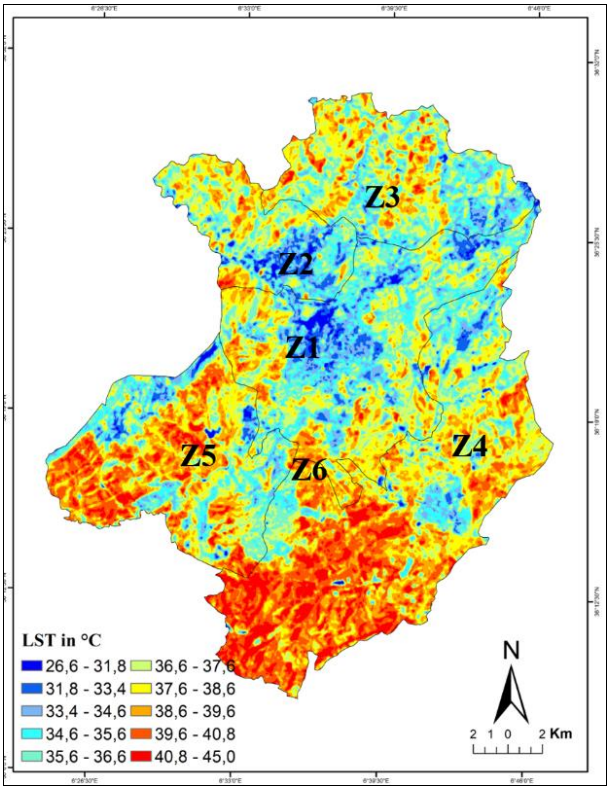

Fig. 4. LST mapping with a classification of 10 classes.

The surface temperature of the rivers and lakes are low compared to the other land cover

types, such as parks and gardens. These mosaic and variety of natural surface coverage lead to the creation of cool areas in a multitude of specific parts of the city [54] such as Z2 where the temperature value may down and reach 26.6°C, as shown in the (Fig.4) presented by blue color.

Based on the findings, it is understood that surface temperature differences in the city contribute to the development of the heat island effect by creating local hottest areas where energy is retained [55]. This energy absorption leads to an "urban heat island" where the part of cities like Z1, Z4, Z5, and Z6 experience higher-than-normal heat temperature.

3.2. Correlation of LST, NDBI and NDVI

The NDBI and NDVI are considered essential indicators generally used for analyzing the correlation between LST, vegetation, and built-up areas [56]. NDBI is commonly applied to extract highly built-up land represented with positive values, and negative values indicate other land cover types. The NDVI is broadly used due to its high sensitivity to chlorophyll.

The (Fig.5) shows the NDBI maps with values ranged from (-0.480 to 0.441).

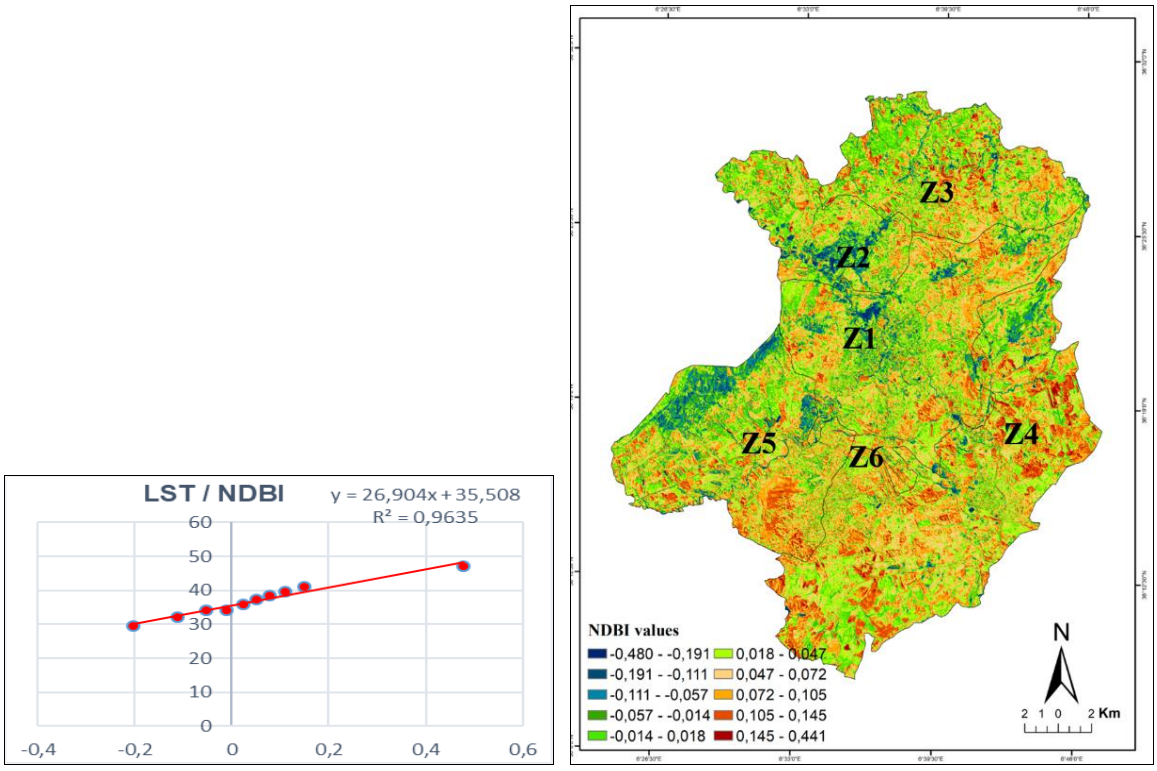

Fig.5. NDBI mapping with a classification of 10 classes and the Pearson's correlation coefficients graph of LST and NDBI

The maximum value is close to 0.441 displayed with shades of orange color. The minimum

values range from (-0.480 to - 0.057) presented with dark blue color, while the average values of NDBI range from (-0.057 to 0.047) with shades of green color. This distribution explains the results obtained before, which generally consider the Z4, Z5, and Z6 as areas with high NDBI values compared with the inner part of Z1 and Z3. As explained before, these areas are commonly covered with rivers and vegetation, have low NDBI. Additionally, the NDBI in some non-urbanized parts of the Z2 is mostly covered with natural land cover, which leads to low values of NDBI. This result confirms the strong correlation between the larger urban built-up land and higher NDBI values, which lead to higher LST [57, 58, 59].

However, the variation of NDVI might cause changes in LST [35, 60]. The spatial distribution of NDVI is illustrated in (Fig.6); the map shows that the NDVI values increase with the dense green areas and vegetation, and with the reduction of built-up areas. Moreover, the high temperature is observed in parts of the city where the vegetation is less dense and more sporadic.

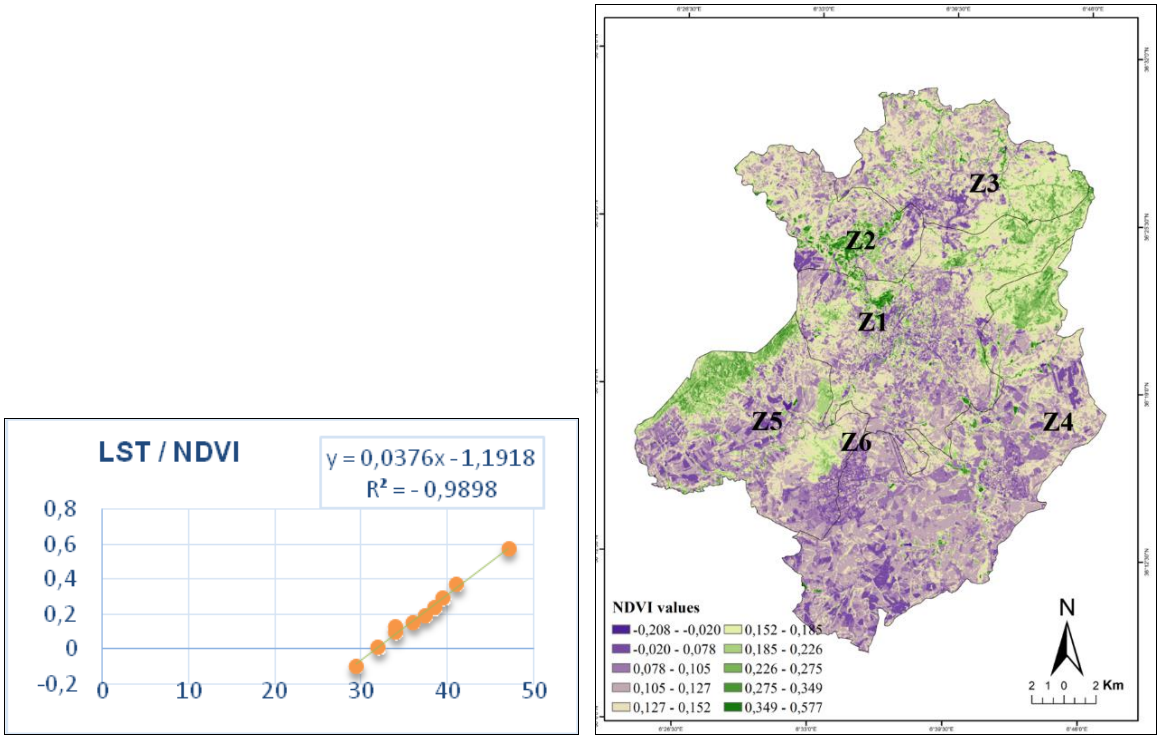

Fig.6. NDVI mapping with a classification of 10 classes and Pearson's correlation coefficients graph of LST and NDVI.

A nonlinear correlation between NDVI and LST was observed with (-0.9898) of Pearson's

coefficient, as shown in the graph in (Fig.6). The NDVI values were ranged from (-0.208 to 0.577). It could be categorized into three groups, based on the LST range: (-0.208-0.105); (0.105-0.226, and (0.226-0.57). Certainly, each NDVI class could be allied to a specific LST range. The first class of LST ranging between (-0.208-0.105) is just about (36°C to 45°C). These temperatures correspond to the areas which contain asphalt surfaces, residential areas with bitumen-flat roofs, shown with purple color in (Fig.6). For the second class of NDVI (0.105-0.226), the LST ranges from (34°C to 36°C). This class matches to the urban areas with suitable amount of vegetation. Several surrounding areas of agricultural lands are also considered in this class as presented by light green color. The NVDI value becomes close to (0.577) in areas that are near to the forests with dense vegetation, showed with bright green color. The reason above these results came mainly from the surface storing heat structural change and evapotranspiration of vegetation, which influences the surface radiation temperature.

3.3. Correlation of LST and topography

The topography is an important factor which can intensify or moderate surface temperature. A negative correlation confirms the well-known relationship between temperature and topography [61, 62]. The LST decreases with an increase in elevation. By contrast, the correlation is linear, while the latter was stronger for the nighttime than for the daytime [63]. In this study, the result highlights a slight difference in this correlation (Fig.7).

The positive correlation was obtained on the surfaces of rivers and some part of green areas, which play a role in the energy fluxes exchange between the surface and the atmosphere [61]; where a low values in elevation will lead to reducing temperatures such as some parts of Z1, Z2, and Z3 displayed by blue color. This can be attributed to the fact that local elevation is low, the air accumulates and therefore the LST is low. Besides, the areas with high values of elevation are the built-up areas exposed to solar radiation during most of the daytime, and the area that received the highest energy is Z6 with a high value of temperature. Additionally, the exposed rock surfaces would have higher LST, due to higher emissivity, as compared with dry soil and vegetation areas.

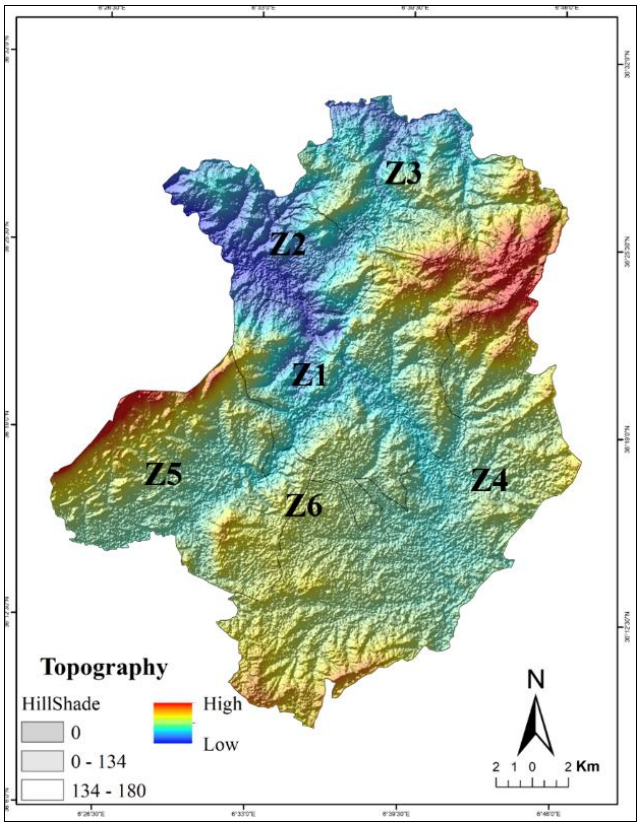

Fig.7.Topograpgy of studied area mapped and shaded

However, a negative correlation between LST and elevation has been observed in high altitudes correspond to the outer part of Z3 and Z5. Also, the high value in elevation with red color represents the lowest temperature, where the vegetation tends to be vertically organized [64]. These findings confirm that LST is influenced by some local parameters such as solar radiation, land surface properties and vegetation in addition to the effect of elevation.

3.4. Detection and analysis of hot-spots

The hot-spots have been defined as the pixel ranged from (30.1°C to 41.4°C) which remains in the higher temperature range as shown in (Fig.8).

Three classes were identified namely; a class represents the slight warm temperature ranged from (30.1°C to 34.6°C) with light yellow color, a class represents warm temperature ranged from (34.6°C to 37.1°C) with an orange color and the last class represents the very hot temperature (37.1°C to 41.4°C) with red color. The result shows that hot-spots were detected in urban areas [65], generally considered as areas with high NDBI and low vegetation which confirm the results obtained before. Also, these hot-spots were correlated to tall residential

buildings with almost 0.379% of bitumen flat-roofs who stores heat, which corroborates the results of [52] and intensify the UHI [66] such as Z1, Z4, Z5 and Z6. Accordingly, the detection of hot-spots helps to determine areas of priority for the implementation of mitigation and adaptation strategies [67].

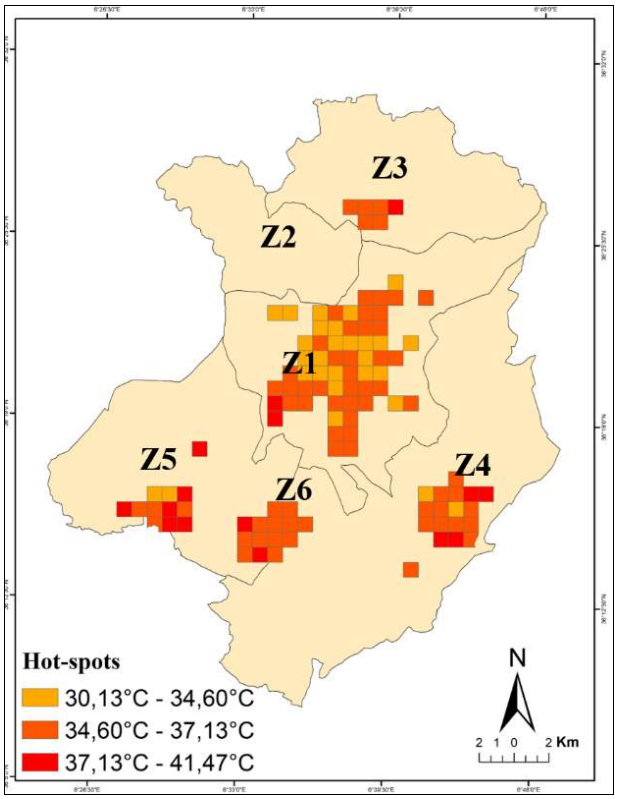

Fig.8. Hot-spots map

3.5. Creation of UCI using GR/UGI ratio (0.0063 reduces 1, 24°C)

In order to quantify the UGI density, the class of non-vegetation represents 80% of the studied area, while the UGI density calculated by the equation (9) represents 19.90%. It includes the sparse and dense vegetation classes. They are respectively 9.12% and 10, 86% of the studied area. According to these values, the analysis revealed a lack of UGI which is correlated to the high values of LST and the formation of UHI [68].

However, increasing UGI is one way to improve the microclimate in high-density cities and reduces surface temperature [69, 70]. It could effectively cool urban surfaces by 20°C [71], particularly in a hot and dry climate [53]. The study of Boudjellal and Bourbia [72] confirmed that planting density is the main factor of the cooling efficiency of vegetation cover in hot and dry environment.

In this regard, using the GR/UGI ratio (0.0063 reduces 1.24°C) has significantly affected the surface temperature distribution and UHI intensity [73]. The new raster values of (UCI) temperature calculated by equation (9) were summarized in (Table 3).

Table 3. New raster values of UCI temperature

Zones	Ratio Abt/Ac (m^2)	CI temperature (degree)
Z1	0.0103	2.02°C
Z3	0.0152	2.99°C
Z4	0.0287	5.64°C
Z5	0.0117	2.30°C
Z6	0.0359	7.06°C
Total	0.1018	20.01°C

The results showed that the average UCI temperature is 4.0°C. The surface temperature decreased by 2.02°C in Z1, by 2.99°C in Z3, 5.64°C in Z4, by 2.30°C in Z5, and it was decreased by 7.06°C in Z6. A non-supervised classification of these values was mapped as shown in (Fig.9).

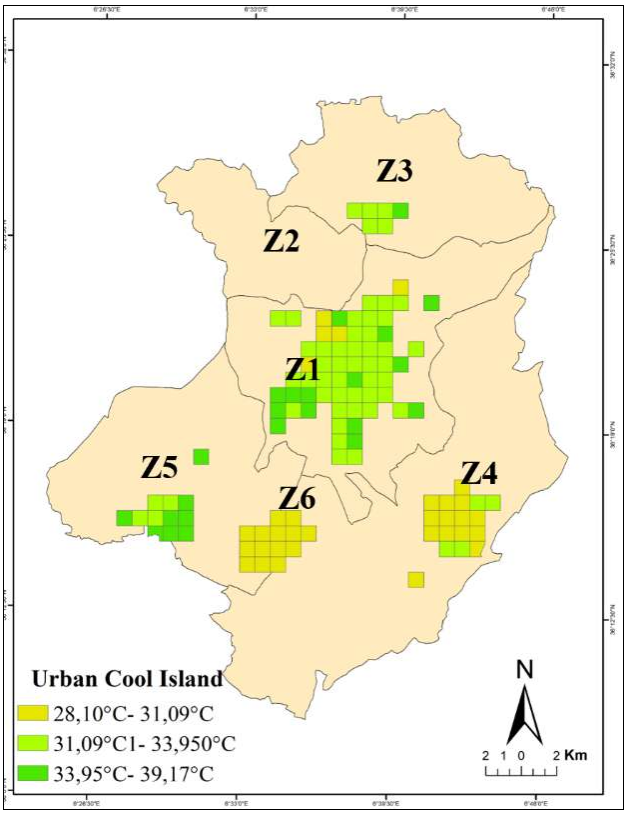

Fig.9. UCI temperature map

These results are consistent with similar studies that show the significant effect of GR on UHI intensity. It has been found that green roofs accounting only 5% of the total area of the city, reduced the temperature in the lower boundary layer by up 0.5°C [74]. Another research conducted in a large urban area of Chicago, showed that daytime roof surface temperature reduced linearly from 0.75 °C to 3.25°C as the green roof ratio increased from 25% to 100% [75]. Besides, our result confirms results from previous studies in similar geographical areas, which have pointed out the effect of diurnal UCI on LST in an arid and semi-arid climate [76, 77, 78].

From the results presented, we conclude that GR has an importance in the increase of UGI density, presenting relatively high heat island mitigation potential. However, the effect of UCI/GR and its characteristics in semi-arid environments still need to be better quantified and understood.

4. CONCLUSION

In a context of climate change, the effects of urban heat islands (UHI) can be broadly intensified and heat stress is expected to progressively increase in urban areas. Planning adapted to climate has become an imperatively challenge for sustainable cities. The Urban Green Infrastructures (UGI) with the presence of Green Roof (GR) are commonly reported to mitigate UHI as the most effective strategies for cooling the urban environment. From the results conducted on the microscale of Constantine city, the impact of the GR/UGI ratio with 0.0063 reduced the average air temperature of 1.24°C during day-time. This study, tried to examine and evaluate the large-scale effect of the mentioned ratio on UHI moderation, creating Urban Cool Island (UCI).

The study conducted in a semi-arid urban area of Constantine, characterized by high intensity solar radiation in summer. A satellite image has been used to estimate surface temperatures and urban variations including NDVI, NDBI and topography. The analysis indicated that LST is influenced by some local parameters such as solar radiation, land surface properties, vegetation surfaces and topography. The higher LST was marked in the rock surfaces exposed to the sun most of day and the dark asphalt covering most urban area acts as heat trap causing

over heating instead of reflecting the solar energy back to space. In addition, these areas have the high values of NDBI and suffer from lack of vegetation, which increase the dryness of the air.

The result of the correlation between vegetation index (NDVI) and LST was negative with value of R^2=-0.9898. As expected, the existing area of vegetation, result in the decrease of LST with 19.90% density of studied area. This suggests that incorporating vegetation using the GR/UGI ratio mitigate UHI in a semi-arid environment. The results show that surface temperature has decreased by 4.0°C of the studied area, creating UCI.

Thus, the findings presented in this paper provide information for urban planners seeking to create a favorable microclimate through vegetation management. Besides, creating UCI for urban areas showed great opportunities for supporting decision makers on specific actions towards a truly sustainable city.

5. REFERENCES

[1] Oke, T. R. (1982). The energetic basis of the urban heat island. *Quarterly Journal of the Royal Meteorological Society,* 108(455), 1-24.

[2] Santamouris, M., Papanikolaou, N., Livada, I., Koronakis, I., Georgakis, C., Argiriou, A., & Assimakopoulos, D. N. (2001). On the impact of urban climate on the energy consumption of buildings. *Solar energy*, 70(3), 201-216

[3] Oke, T. R. (2002). *Boundary layer climates*: Routledge.

[4] Akbari, H., Rose, L. S., & Taha, H. (2003). Analyzing the land cover of an urban environment using high-resolution orthophotos. *Landscape and urban planning*, 63 (1), 1-14.

[5] EPA, U. (2008). Reducing urban heat islands: compendium of strategies. Heat Island Reduction Activities, 1-23.

[6] Liu & Zhang, 2011; Liu, L., & Zhang, Y. (2011). Urban heat island analysis using the Landsat TM data and ASTER data: A case study in Hong Kong. *Remote Sensing*, 3(7), 1535–1552.

[7] Weng, 2010 Weng, Q. (2010). Remote sensing and GIS integration: Theories, methods, and applications. New York: McGraw Hill Professional.

[8] An urban heat island study in Nanchang City, China based on land surface temperature and social-ecological variables. *Sustainable cities and society*, 32, 557-568

[9] Yang, J., Jin, S., Xiao, X., Jin, C., Xia, J. C., Li, X., & Wang, S. (2019). Local climate zone ventilation and urban land surface temperatures: Towards a performance-based and wind-sensitive planning proposal in megacities. *Sustainable Cities and Society*, 47, 101487.

[10] Chen, X., & Zhang, Y. (2017). Impacts of urban surface characteristics on spatiotemporal pattern of land surface temperature in Kunming of China. *Sustainable Cities and Society*, 32, 87-99.

[11] Dwivedi, A., & Khire, M. V. (2018). Application of split-window algorithm to study Urban Heat Island effect in Mumbai through land surface temperature approach. *Sustainable Cities and Society*, 41, 865-877.

[12] Madanian, M., Soffianian, A. R., Koupai, S. S., Pourmanafi, S., & Momeni, M. (2018). The study of thermal pattern changes using Landsat-derived land surface temperature in the central part of Isfahan province. *Sustainable cities and society*, 39, 650-661.

[13] Yang, J., Sun, J., Ge, Q., & Li, X. (2017). Assessing the impacts of urbanization-associated green space on urban land surface temperature: A case study of Dalian, China. *Urban Forestry & Urban Greening,* 22, 1-10

[14] Cai, Z., Han, G., & Chen, M. (2018). Do water bodies play an important role in the relationship between urban form and land surface temperature? *Sustainable cities and society*, 39, 487-498

[15] Santamouris, M., Ding, L., Fiorito, F., Oldfield, P., Osmond, P., Paolini, R., ... & Synnefa, A. (2017). Passive and active cooling for the outdoor built environment–Analysis and assessment of the cooling potential of mitigation technologies using performance data from 220 large scale projects. *Solar Energy*, 154, 14-33.

[16] Aflaki, A., Mirnezhad, M., Ghaffarianhoseini, A., Ghaffarianhoseini, A., Omrany, H., Wang, Z. H., & Akbari, H. (2017). Urban heat island mitigation strategies: A state-of-the-art review on Kuala Lumpur, Singapore and Hong Kong. *Cities*, 62, 131-145.

[17] He, B. J. (2019). Towards the next generation of green building for urban heat island mitigation: Zero UHI impact building. *Sustainable Cities and Society*, 50, 101647

[18] Guo, A., Yang, J., Xiao, X., Xia, J., Jin, C., & Li, X. (2020). Influences of urban spatial form on urban heat island effects at the community level in China. *Sustainable Cities and Society*, *53*, 101972

[19] Yang, J., Jin, S., Xiao, X., Jin, C., Xia, J. C., Li, X., & Wang, S. (2019). Local climate zone ventilation and urban land surface temperatures: Towards a performance-based and wind-sensitive planning proposal in megacities. *Sustainable Cities and Society*, 47, 101487

[20] Yu, C., & Hien, W. N. (2006). Thermal benefits of city parks. *Energy and buildings*, 38(2), 105-120.

[21] Nasrallah, H. A., Brazel, A. J., & Balling Jr, R. C. (1990). Analysis of the Kuwait City urban heat island. *International Journal of Climatology*, *10*(4), 401-405.

[22] Wen, L. J., Lü, S. H., Chen, S. Q., Meng, X. H., & Bao, Y. (2005). Numerical simulation of cold island effect in Jinta Oasis summer. *Plateau Meteorology*, 24(6), 865-871.

[23] Li, S., Mo, H., & Dai, Y. (2011). Spatio-temporal pattern of urban cool island intensity and its eco-environmental response in Chang-Zhu-Tan urban agglomeration. *Communications in Information Science and Management Engineering*, *1*(9).

[24] Steinecke, K. (1999). Urban climatological studies in the Reykjavık subarctic environment, Iceland. *Atmospheric environment*, 33(24-25), 4157-4162.

[25] Keramitsoglou, I., Kiranoudis, C. T., Ceriola, G., Weng, Q., & Rajasekar, U. (2011). Identification and analysis of urban surface temperature patterns in Greater Athens, Greece, using MODIS imagery. *Remote Sensing of Environment*, 115(12), 3080-3090.

[26] Skinner, C., & Bruse, M. (2000). Rooftop greening and local climate: A case study in Melbourne. *Biometeorology and Urban Climatology at the Turn of the Millennium, WMO*, 21-25.

[27] Peng, L. L.,&Jim, C. (2013). Green-roof effects on neighborhood microclimate and human thermal sensation. *Energies,* 6(2), 598-618.

[28] Ambrosini, D., Galli, G., Mancini, B., Nardi, I., & Sfarra, S. (2014). Evaluating mitigation effects of urban heat islands in a historical small center with the ENVI-Met® climate model. *Sustainability,* 6(10), 7013-7029.

[29] Wang, Y., Berardi, U., & Akbari, H. (2016). Comparing the effects of urban heat island mitigation strategies for Toronto, Canada. *Energy and buildings*, 114, 2-19.

[30] Sahnoune, S., &Benhassine, N. (2017). Quantifying the impact of green-roofs on urban heat island mitigation. *International Journal of Environmental Science and Development*, 8(2), 116.

[31] Oke, T. R. (2006). Towards better scientific communication in urban climate. *Theoretical and Applied Climatology*, 84 (1-3), 179-190.

[32] Nichol, J. E. (1994). A GIS-based approach to microclimate monitoring in Singapore's high-rise housing estates. Photogrammetric *Engineering and Remote Sensin*g,60, 1225–1232.

[33] Weng, Q., Lu, D., &Schubring, J. (2004). Estimation of land surface temperature–vegetation abundance relationship for urban heat island studies. *Remote sensing of Environment*, 89(4), 467-483

[34] Sobrino, J. A., Jimenez-Munoz, J. C., & Paolini, L. (2004). Land surface temperature retrieval from LANDSAT TM 5. *Remote Sensing of environment*, 90(4), 434-440.

[35] Carlson, T. N., Gillies, R. R., & Perry, E. M. (1994). A method to make use of thermal infrared temperature and NDVI measurements to infer surface soil water content and fractional vegetation cover. *Remote sensing reviews,* 9(1-2), 161-173.

[36] Purevdorj, T., Tateishi, R., Ishiyama, T., & Honda, Y. (1998). Relationships between percent vegetation cover and vegetation indices. *International Journal of Remote Sensing,* 19(18), 3519-3535

[37] Zha, Y., Gao, J., & Ni, S. (2003). Use of normalizeddifference built-up index in automatically mapping urban areas from TM imagery. *International Journal of Remote Sensing,* 24(3), 583-594.

[38] Landsat Project Science Office (2002). Landsat 7 Science Data User's Handbook. URL:https://www.gsfc.nasa.gov/IAS/handbook/handbook_toc.html, Goddard Space Flight Center, NASA, Washington, DC (last date accessed: 24 September 2016).

[39] Valor, E., & Caselles, V. (1996). Mapping land surface emissivity from NDVI: Application to European, African, and South American areas. *Remote sensing of Environment,* 57(3), 167-184.[32] Artis, D. A., &Carnahan, W. H. (1982). Survey of

emissivity variability in thermography of urban areas. *Remote Sensing of Environment*, 12,313– 329.

[40] Artis, D. A., &Carnahan, W. H. (1982). Survey of emissivity variability in thermography of urban areas. *Remote Sensing of Environment*, 12,313– 329.

[41] Hais, M., & Kučera, T. (2009). The influence of topography on the forest surface temperature retrieved from Landsat TM, ETM+ and ASTER thermal channels. *ISPRS Journal of Photogrammetry and Remote Sensing*, 64(6), 585-591

[42] Mayer, H., & Hoppe, P. (1987). Thermal comfort of man in different urbanenvironments. Theoretical and Applied Climatology, 38, 43–49.

[43] Huynh, C., & Eckert, R. (2012). Reducing heat and improving thermal comfort through urban design-A case study in Ho Chi Minh city. *International Journal of Environmental Science and Development,* 3(5), 480.

[44] Noro, M., Busato, F., & Lazzarin, R. (2014). UHI effect in the city of Padua: simulations and mitigation strategies using the Rayman and envimet model. *Geographia Polonica,* 87(4), 517-530.

[45] O'Malley, C., Piroozfarb, P. A., Farr, E. R., & Gates, J. (2014). An investigation into minimizing urban heat island (UHI) effects: A UK perspective. *Energy Procedia,* 62, 72-80.

[46] Chandramathy, A. I., & Arch, M. (2014, December). Green space factor in modifying the microclimates in a neighbourhood: theory and guidelines. In *Proceedings of the 30th International PLEA Conference, Ahmedabad, India* (pp. 16-18).

[47] Ouameur, F. A. (2007). Morphologie urbaine et confort thermique dans les espaces publics. Étude comparative entre trois tissus urbains de la ville de Québec *(Doctoral dissertation, Université Laval).*

[48] Yi, C. Y., & Peng, C. (2017). Correlating cooling energy use with urban microclimate data for projecting future peak cooling energy demands: Residential neighbourhoods in Seoul. *Sustainable Cities and Society*, 35, 645-659.

[49] Luo, H., Huang, B., Liu, X., & Zhang, K., 2011). Green roof assessment by GIS and google earth. *Procedia Environmental Sciences*, 10, 2307-2313.

[50] Sartz, R. S. (1972). *Effect of topography on microclimate in southwestern Wisconsin* (Vol. 74). North Central Forest Experiment Station, Forest Service, US Department of Agriculture

[51] Rizwan, A. M., Dennis, L. Y., & Chunho, L. I. U. (2008). A review on the generation, determination and mitigation of Urban Heat Island. *Journal of Environmental Sciences*, 20(1), 120-128.

[52] Oke, T. R., & Cleugh, H. A. (1987). Urban heat storage derived as energy balance residuals. *Boundary-Layer Meteorology*, 39(3), 233-245.

[53] Taha, H. (1997). Urban climates and heat islands; albedo, evapotranspiration, and anthropogenic heat. *Energy and buildings*, 25(2).

[54] Norton, B. A., Coutts, A. M., Livesley, S. J., Harris, R. J., Hunter, A. M., & Williams, N. S. (2015). Planning for cooler cities: A framework to prioritise green infrastructure to mitigate high temperatures in urban landscapes. *Landscape and urban planning*, 134, 127-138.

[55] Rosenzweig, C., Solecki, W., & Slosberg, R. (2006). Mitigating New York City's heat island with urban forestry, living roofs, and light surfaces. *A report to the New York State Energy Research and Development Authority*.

[56] Jamei, Y., Rajagopalan, P., & Sun, Q. C. (2019). Spatial structure of surface urban heat island and its relationship with vegetation and built-up areas in Melbourne, Australia. *Science of the Total Environment*, 659, 1335-1351.

[57] Li, H., & Liu, Q. (2008, December). Comparison of NDBI and NDVI as indicators of surface urban heat island effect in MODIS imagery. In *International conference on earth observation data processing and analysis (ICEODPA) (Vol. 7285, p. 728503). International Society for Optics and Photonics.*

[58] Chen, L., Li, M., Huang, F., & Xu, S. (2013, December). Relationships of LST to NDBI and NDVI in Wuhan City based on Landsat ETM+ image. In *2013 6th International Congress on Image and Signal Processing* (CISP) (Vol. 2, pp. 840-845). IEEE.

[59] Morabito, M., Crisci, A., Messeri, A., Orlandini, S., Raschi, A., Maracchi, G., & Munafò, M. (2016). The impact of built-up surfaces on land surface temperatures in Italian urban areas. *Science of the Total Environment*, 551, 317-326.

[60] Goetz, S. (1997). Multi-sensor analysis of NDVI, surface temperature and biophysical variables at a mixed grassland site. *International Journal of Remote Sensing*, 18(1), 71-94.

[61] Stroppiana, D., Antoninetti, M., & Brivio, P. A. (2014). Seasonality of MODIS LST over Southern Italy and correlation with land cover, topography and solar radiation. *European Journal of Remote Sensing*, 47(1), 133-152.

[62] Mathew, A., Khandelwal, S., & Kaul, N. (2016). Spatial and temporal variations of urban heat island effect and the effect of percentage impervious surface area and elevation on land surface temperature: Study of Chandigarh city, India. *Sustainable Cities and Society*, 26, 264-277.

[63] Phan, T., Kappas, M., & Tran, T. (2018). Land Surface Temperature Variation Due to Changes in Elevation in Northwest Vietnam. *Climate,* 6(2), 28.

[64] Bertoldi, G., Notarnicola, C., Leitinger, G., Endrizzi, S., Zebisch, M., Della Chiesa, S., & Tappeiner, U. (2010). Topographical and ecohydrological controls on land surface temperature in an alpine catchment. *Ecohydrology: Ecosystems, Land and Water Process Interactions, Ecohydrogeomorphology*, 3(2), 189-204.

[65] Jusuf, S. K., Wong, N. H., Hagen, E., Anggoro, R., & Hong, Y. (2007). The influence of land use on the urban heat island in Singapore. *Habitat international*, 31(2), 232-242

[66] Yang, F., Lau, S. S., & Qian, F. (2011). Urban design to lower summertime outdoor temperatures: An empirical study on high-rise housing in Shanghai. *Building and Environment*, 46(3), 769-785.

[67] Wang, J., Zhan, Q., & Guo, H. (2016). The morphology, dynamics and potential hotspots of land surface temperature at a local scale in urban areas. *Remote Sensing*, 8(1), 18.

[68] Grimmond, C. S. B., & Oke, T. R. (1991). An evapotranspiration-interception model for urban areas. *Water Resources Research,* 27 (7), 1739-1755.

[69] Bowler, D. E., Buyung-Ali, L., Knight, T. M., & Pullin, A. S. (2010). Urban greening to cool towns and cities: A systematic review of the empirical evidence. *Landscape and urban planning*, 97(3), 147-155.

[70] Andersson-Sköld, Y., Thorsson, S., Rayner, D., Lindberg, F., Janhäll, S., Jonsson, A., ... &Granberg, M. (2015). An integrated method for assessing climate-related risks and

adaptation alternatives in urban areas. *Climate Risk Management*, 7, 31-50.

[71] Armson, D., Stringer, P., & Ennos, A. R. (2012). The effect of tree shade and grass on surface and globe temperatures in an urban area. *Urban Forestry & Urban Greening*, 11(3), 245-255.

[72] Boudjellal, L., & Bourbia, F. (2018). An evaluation of the cooling effect efficiency of the oasis structure in a Saharan town through remotely sensed data. *International Journal of Environmental Studies*, 75(2), 309-320

[73] Saito, I., Ishihara, O., & Katayama, T. (1990). Study of the effect of green areas on the thermal environment in an urban area. *Energy and buildings*, 15(3-4), 493-498.

[74] Bass, B., Krayenhoff, S., Martilli, A., & Stull, R. (2002). Mitigating the urban heat island with green roof infrastructure. Urban Heat Island Summit: Toronto.

[75] Sharma, A., Conry, P., Fernando, H. J. S., Hamlet, A. F., Hellmann, J. J., & Chen, F. (2016). Green and cool roofs to mitigate urban heat island effects in the Chicago metropolitan area: Evaluation with a regional climate model. *Environmental Research Letters*, 11(6), 064004.

[76] Rasul, A., Balzter, H., & Smith, C. (2015). Spatial variation of the daytime Surface Urban Cool Island during the dry season in Erbil, Iraqi Kurdistan, from Landsat 8. Urban climate, 14, 176-186.

[77] Frey, C. M., Rigo, G., & Parlow, E. (2009). Investigation of the daily Urban Cooling Island (UCI) in two coastal cities in an arid environment: Dubai and Abu Dhabi (UAE). *City*, 81(2.06).

[78] Abdullah, H. (2012). The Use of Landsat 5 TM Imagery to Detect Urban Expansion and Its Impact on Land Surface Temperatures in The City of Erbil, Iraqi Kurdistan. MSc, University of Leicester, 7(12), 3209-3241.

How to cite this article:
Sahnoune S, Benhassine N, Bourbia F, Hadbaoui H. Quantifying the effect of green-roof and urban green infrastructure ratio on urban heat island mitigation- semi-arid climate. J. Fundam. Appl. Sci., 2021, *13(1), 199-224.*